# Relationship between soil carbon sequestration and the ability of soil aggregates to transport dissolved oxygen

Xiaoxian Zhang[1], Andrew S. Gregory[1], William R. Whalley[1], Kevin Coleman[1], Andrew L. Neal[2], Aurelie Bacq-Labreuil[3], Sacha J. Mooney[3], John W Crawford[4], Kenichi Soga[5], Tissa H. Illangasekare[6]

[1] Department of Sustainable Agricultural Sciences, Rothamsted Research, Harpenden, AL5 2JQ, UK.

[2] Sustainable Agriculture Sciences, Rothamsted Research, North Wyke, EX20 2SB, UK

[3] Division of Agriculture & Environmental Sciences, School of Biosciences, University of Nottingham, Sutton Bonington Campus, Leicestershire LE12 5RD, UK.

[4] Adam Smith Business School, University of Glasgow, West Quadrangle, Glasgow. G12 8QQ. UK

[5] Department of Civil and Environmental Engineering, University of California–Berkeley, Berkeley, CA 94720, USA.

[6] Centre for Experimental Study of Subsurface Environmental Processes, Colorado School of Mines, Golden CO, USA

**Abstract**

A key finding in soil carbon studies over the past decade is that soil organic carbon (SOC) stabilization is not controlled by its molecular complexity or adsorption to clay, but by its physicochemical protection including occlusion in aggregates and sorption/precipitation with organo-mineral associations. The organo-mineral complexes and the adsorbed SOC can be dissolved microbially under anoxic conditions, which is an important pathway in carbon cycle but has been overlooked by most carbon models. As organo-mineral associations are reported to form in aerobic conditions and can be lost under anaerobic conditions, there should be a positive correlation between SOC and ability of the aggregates to transport dissolved oxygen. We develop a simulation model to test this using soil structural data from two long-term experiments which naturally created a SOC gradient: One is a winter wheat experiment established in 1843 to compare the effects of different fertilizations on the yield of winter wheat and the other one is a ley-arable experiment established in 1948 to investigate the consequence of cropping system changes for ecological yield. Aggregates from different treatments on the two experiments were scanned using X-ray Computed Tomography to simulate oxygen transport using a pore-scale model. We compared porosity and diffusion coefficient of all aggregates and linked them to soil organic carbon measured from the two experiments. The agronomic practice changes which occurred 67 or 172 years ago substantially reshaped the intra-aggregate structure (<2mm), and the accrual of SOC is positively correlated with diffusion coefficient of the aggregates to transport oxygen. However, the diffusion coefficient increases with SOC asymptotically, plateauing when SOC exceeds a threshold value. We also found the diffusion coefficient of the aggregates in chemically fertilized soils trended with their porosity approximately in the same way, deviating from those for other non-cropped treatments or fertilized with farmyard manure.

***Key words****: Rothamsted long-term experiments*; soil organic carbon; aggregates, transport properties; *pore-scale simulation*.

## 1. Introduction

Hydrological and biogeochemical functions of terrestrial ecosystems are modulated by their hierarchically structured soils (Young and Crawford, 2004). Although the feedbacks between soil structure and biogeochemical reactions have been well documented (Young and Crawford, 2004; Rabot et al., 2018), the underlying mechanisms are not well understood due to the opaque nature of the soils (Baveye et al., 2018). Application of imaging technologies over the past decades has helped break this barrier, finding, for example, exoenzymes are not uniformly distributed but clustered around a specific range of pores (Guber et al., 2018; Kraychenko et al., 2019; Lucas et al., 2020). As enzyme diffusion in soil is slow (Rothman and Forney, 2007; Boudreau et al., 2008), these findings indicate that soil organic matter (SOM) decomposition is limited to the regions proximal to these pores, which has important implications for soil carbon modelling (van Groenigen et al., 2017; Poulton et al., 2018; Chenu et al., 2019; Soussana et al., 2019; Sykes et al., 2020). This is also corroborated by recent findings that soil carbon depends only weakly on clay content while is correlated significantly with Fe and Al across a wide range of ecosystems (Rasmussen et al., 2018).

SOM retained in soil is the consequence of a multitude of interactive physicochemical and biological processes mediated by soil structure (Six et al., 2002). Since a large fraction of soil pores are devoid of microbes and SOM (Nunan et al., 2003; Li et al., 2018), carbon metabolization is controlled by its accessibility to microbes rather than by its chemical complexity as biogeochemical reactions proceed only at hydrated sites with microbes and substrates coexisting (Schmidt et al., 2011; Dungait et al., 2012; Sulman et al., 2014; Lehmann and Kleber, 2015). This implicates that using effective reaction rates by averaging the microscopic processes out, as being used in most pool-based models, is inadequate to describe the volumetric-average biogeochemical reactions (Manzoni et al., 2012; Chakrawal et al., 2020), and improved models are needed to reduce the uncertainties in predicting the feedbacks between SOM and climate change (Schmidt et al., 2011; Lehmann et al., 2020). One such approach is the reactive continuum model by representing the decay rate of the chemically and spatially heterogeneous SOM as a random number rather than constant (Bolker et al., 1998; Rothman and Forney, 2007).

Both pool-based and reactive continuum models oversimplify the extremely complex system with the aim of predicting long-term soil organic carbon (SOC) change. They describe the combined impact of climatic and edaphic factors collectively using a moisture function and a temperature function assuming the impacts of soil water and temperature are multiplicative (Skopp et al., 1990; Davidson et al., 2006; Davidson et al., 2012; Moyano et al., 2013). They do not, however, explicitly consider constraints of nutrients and soil structure, despite the consensus that a change in soil structure reshapes soil physicochemical environments, thereby altering the reactivity continuum (Baldock and Skjemstad, 2000). This in one reason behind the uncertainties in predicting the feedback between soil carbon and climate change (Luo et al., 2016). Improving SOM modelling thus requires a better understanding of the underlying mechanisms (Luo et al., 2020; Smith et al., 2020), and one approach is to incorporate the microscopic processes (Ebrahimi and Or, 2016; Yan et al., 2018; Ghezzehei et al., 2019).

A key finding over the past two decades is that SOM persistence in soil is not controlled by its chemical complexity but by its protection in the heterogeneous physical and chemical environments (Schmidt et al., 2011; Yu et al., 2017). Large and complex macromolecules recalcitrant to microbial decomposition are found to account for only a small fraction of SOM, and the majority of stable SOM are small molecules occluded in aggregates and sorbed by metal oxides, especially iron and manganese oxides (Sutton and Sposito, 2005; von Lutzow et al., 2006; Kogel-Knabner et al., 2008; Jones and Singh, 2014). Organo-mineral complexities are normally formed under aerobic conditions (Chen et al., 2020; Yuan et al., 2020), and they can be dissolved microbially when the soils become anaerobic (Knorr, 2013; Zhao et al., 2017). This is an important pathway in carbon cycle and has significant implications for long-term stability of SOM (Hemingway et al., 2019). It contradicts the traditional view of the pool-based models that oxygen limitation suppresses SOM decomposition due to the kinetic and thermodynamic constraints on microbial metabolism

(Freeman et al., 2001; LaRowe and Van Cappellen, 2011; Huang et al., 2020). Increasing evidence over the past few years has shown that, while anaerobic conditions reduce decomposition of organic litter (Zhao et al., 2020), microbial dissimilatory reduction could dissolve the organo-mineral associations and mobilize the older carbons as a result (Knorr, 2013; Chen et al., 2020). When soil becomes aerobic, such carbon can be quickly oxidized microbially, increasing gas emissions as a result (Wang et al., 2017; Chen et al., 2020).

The effects of oxygen limitation on SOM in wetlands and marine sediments have been well documented (Freeman et al., 2001; Arndt et al., 2013), but it is less known that anoxia is also prevalent in dry soil due to the hierarchical structure of soils (Keiluweit et al., 2016). For example, it was found in a tropical upland soil that carbon mobilised from iron oxide dissolution following microbially-mediated reduction accounted for more than 40% of total oxidized carbon (Dubinsky et al., 2010). Even in partly saturated rhizosphere, an increase in microbial consumption of oxygen could make the rhizosphere increasingly anoxic, dissolving the organo-mineral complexes (Keiluweit et al., 2015). Therefore, there is a trade-off between aerobic and anaerobic conditions in their impacts on SOM. The imbalance between microbial consumption of oxygen and the limited ability of soil to dissolve and transport oxygen could lead to prevalent development of anoxic spots, particularly inside soil aggregates. This could have a profound consequence for SOM dynamics (Sexstone et al., 1985; Hall and Silver, 2015; Keiluweit et al., 2016; Huang et al., 2020; Neal et al., 2020), and has been postulated one of the mechanisms underlying the surprising acceleration of $N_2O$ emissions over the last 10 years (Harris et al., 2021).

Organo-mineral associations are formed under aerobic conditions and are the dominant carbon stock in some systems (DeGryze et al., 2004; Chen et al., 2020). Hence, we conjecture that there should be a positive correlation between stable SOM and the ability of soil aggregates to transport oxygen as long-term stabilization of the organo-mineral complexities needs the aggregates to be more aerobic. Testing this, however, needs long-term experiments with SOM gradients as carbon stabilization in soil is a slow process and could take centuries to reach new equilibria following agronomic practice changes (Poulton et al., 2018; Totsche et al., 2018).

In this paper, we calculate the relationship between soil organic carbon (SOC) and the ability of aggregates to transport dissolved oxygen based on two long-term experiments at Rothamsted Research. Aggregates in soil cores taken from plots under different treatments were scanned using X-ray Computed Tomography (CT), and their effective diffusion coefficient for dissolved oxygen was calculated based on pore-scale simulations assuming the aggregate was saturated as this is the most anoxic condition. We then compared how the agronomic management changes made 67 or 172 years ago reshaped the intra-aggregate structure and its consequence for SOC stabilization.

## 2. Materials and methods

### 2.1. The long-term experiments

The experiments, established from the 1840s onwards, at Rothamsted Research in the UK are the longest-running agricultural experiments in the world that are still in operation. Details of all experiments are available online at the Electronic Rothamsted Archive (e-RA) website (http://www.era.rothamsted.ac.uk). We focused on the two experiments described in the following two sections. Soil type and texture on the two experiments are the same, being predominantly clay loam and classified as Chromic Luvisol (FAO classification). The mean annual rainfall and temperature on the two sites are 701 mm and 10.1 °C respectively. The top 0-23 cm soil contains 25% sand, 50% silt and 25% clay, and the average particle density was 2.56 g/cm$^3$ (Gregory et al., 2010). We used data on soil organic carbon from the e-RA.

#### 2.1.1 The Broadbalk Winter Wheat experiment

The Broadbalk Winter Wheat experiment started in 1843 (Latitude 51° 48’ 34.44” N; Longitude 0° 21’ 22.76” W) aiming to compare the impact of different chemical fertilizations and farmyard manure on the yield of winter wheat, with an unfertilized treatment as the control (Figure S1). There have been a few changes since its inception to represent the changes to farming in the UK, and further details are available in the literature (Blair et al., 2006; Watts et al., 2006) and online via the above link. The supplementary materials depict the site layout and the fertilization history. In brief, the initial arrangement of the experiment was in 19 strips with each associated with a specific fertilization; a small part on the west edge of the site was taken out of cultivation in 1882 and has since returned to woodland. The pH is controlled by liming to stay at 7-7.5.

Soil samples were taken from four plots (Figure S1). One plot is applied with farmyard manure since 1843 at an annual rate of 35 t/ha (referred as to FYM hereafter); one plot is applied with inorganic fertilizers (144 kg/ha nitrogen, 35 kg/ha phosphorus, 90 kg/ha potassium and 12 kg/ha magnesium, annually) since 1852 (referred as to N3 hereafter); one plot is fertilized annually with 192 kg/ha of N (96 kg/ha of N 1906–2000), 90 kg/ha of K and 12 kg/ha Mg since 1906 but without P (referred as to No P hereafter); one plot is a control without any kind of fertilization since 1843 (CK). All plots are tilled conventionally. Samples were also taken from the woodland (referred as to woodland hereafter).

**2.1.2. The Highfield Ley-Arable experiment**

The Highfield Ley-Arable experiment is approximately 500 m south of the Broadbalk experiment (Figure S2), and the site had been under permanent grass at least since 1838. It was established in 1948 to examine the impact of land management on soil carbon and ecological yield (Gregory et al., 2016). There are six ley-arable treatments, comprising treatments under permanent grass, permanent arable and ley-arable treatments, each in a 7 m × 50 m plot, arranged in a randomly designed block (with four blocks). After a ploughing in 1959, a plot of land of approximately 900 $m^2$ on the edge of the site has remained permanent bare fallow since by mouldboard ploughing and cultivating annually the top 23 cm of soil 2-4 times annually. Detailed description of the experiment was available online via the above link and in the literature (Gregory et al., 2016; Jensen et al., 2019; Redmile-Gordon et al., 2020). The treatments we studied are permanent grass (predominantly rye grass, *Lolium perenne L.*), continuous arable (winter wheat, *Triticum aestivum L.*) and bare fallow.

**2.2. X-ray Computed Tomography imaging**

Three or four soil cores , 12 cm high and 6.8 cm in diameter, were taken in October 2015 from each treatment on the two experiments. Following a pre-treatment and X-ray imaging (data not presented here), each core was manually broken and passed through sieves (2mm-0.71mm) by horizontally shaking (see Bacq-Labreuilet al (2018) for details). Three aggregates were randomly selected from those retained in the sieves and they were then scanned at resolution of 1.5 μm using the Phoenix Nanotom® (GE Measurement and Control solution, Wunstorf, Germany) under 90 kV and 65 μA. Overall, there were at least nine aggregate replicates for each treatments.

Each image was reconstructed using the datos|x software and then analysed using Image J (Schneider et al., 2012), in which a region of interest (ROI) was cropped out for ease of analysis. As the aggregates were geometrically irregular, the ROI taken from all aggregates was cuboid consisting of 400 x 480 x 650 voxels. The ROIs were segmented using the threshold method presented in Vogel and Kretzschmar (1996); for further details of the imaging processing see Bacq-Labreuilet al al (2018).

**2.2. Pore-scale simulations**

The ability of aggregates to transport oxygen was calculated numerically by mimicking oxygen movement in the pore space. Considering aggregates are mostly anaerobic under saturated conditions, we simulated oxygen diffusion assuming the pore space in each aggregate was fully saturated. We acknowledge that by this approach we do not consider pores smaller than 1.5 μm in the aggregates due to the voxel size. In terms of microbial activity, pores smaller than 1.5 μm are not accessible to microbes (or are severely limited) and their role in microbial reductions is hence insignificant as microbial reductions proceed only at sites with coexistence of cells and substrates. Furthermore, as pore size decreases, the Knudsen number increases and the frictions caused by oxygen collisions with pore walls also increase (Li et al., 2017). Therefore, the pores captured in the images are representative of the ability of the aggregate to transport oxygen and other dissolved substrates which are relevant to microbial activity.

The oxygen movement was simulated using the lattice Boltzmann model developed previously (Zhang et al., 2016b; Li et al., 2018). Details of the method are given in the appendix. In short, for each sample, a concentration gradient was generated in one direction by imposing a high constant concentration on one side and a low constant concentration on its opposite side to drive the oxygen to diffuse; the other four sides were treated as periodic boundaries. Once the diffusion was deemed to have reached steady state, oxygen concentration and diffusive flux in all voxels were sampled, and they were then volumetrically averaged across each section perpendicular to the concentration gradient direction. These bulk average concentrations and diffusive fluxes were assumed to follow Fick's law. For example, when the concentration gradient was generated in the z direction, this means

$$Q_z = -D_e \frac{\partial C}{\partial z} \tag{1}$$

where $Q_z$ is the average diffusive flux in the $z$ direction, $C$ is the average concentration and $D_e$ is the effective diffusion coefficient describing the average ability of the aggregate to transport oxygen in the z direction. At steady state, the mass balance requires $Q_z$ independent of $z$, and the effective diffusion coefficient can thus be calculated from the pore-scale simulation as follows:

$$D_e = \frac{L}{N} \frac{\sum_{i=1}^{N} j_z\left(x_i, y_i, z_i\right)}{C_0 - C_1} \tag{2}$$

where $N$ is the total number of pore voxels, $L$ is the length of the image in the $z$ direction, $j_z(x_i, y_i, z_i)$ is the diffusive flux component in the z direction at the voxel with coordinate $(x_i, y_i, z_i)$, and $C_1$ and $C_0$ are the two constant concentrations imposed on the two sample sides in the z direction. For each sample, we calculated its effective diffusion coefficient in three orthogonal directions aimed to examine anisotropy.

### 2.3. Statistical analysis

Difference in the mean of the variates (n=9-12) between the treatments in each of the two experiments was assessed by analysis of variance (ANOVA). The post-hoc pairwise comparisons of the treatment-means were performed using the Duncan's multiple range test with the difference considered significant at $p < 0.05$. All data were analysed using Matlab.

## 3. Results

Figure 1 shows representative images for aggregates taken from the seven plots and the woodland to visually illustrate how changes in agricultural management and fertilizations have reshaped the intra-aggregate structure. All aggregates show anisotropy to some extent, with the ratio of the least effective diffusion coefficient in one direction to the highest effective diffusion coefficient in other direction varying between aggregates and treatments. However, for all aggregates such ratios were greater than 80%. From the way the aggregates were sampled and scanned, it was impossible to keep their orientation in the field. For each aggregate, we thus used the average of the effective diffusion coefficients in the three orthogonal directions to represent its ability to transport dissolved oxygen. Diffusion of dissolved oxygen in water depends on temperature, and its diffusion coefficient is thus not constant but varies with temperature. To highlight the impact of intra-aggregate structure, in what follows we will normalise the effective diffusion coefficient of all aggregates by diffusion coefficient of dissolved oxygen in water under the same temperature $D$, i.e., $D'=D_e/D$. Such normalization also enables us to extrapolate the results to calculate effective diffusion coefficient of other dissolved substrates in the aggregates. Since the inception of the ley-arable experiment, SOC content in the soil has not yet reached new equilibria with SOC in the arable treatment still steadily declining while in the grassland it is asymptotically increasing; we thus analysed the results obtained from the two experiments separately. Since geometrical results of the images, including the pore-size distributions, Euler numbers and critical pore diameters, have been presented previously (Bacq-Labreuil et al., 2018; Zhang et al., 2021), in what follows we only show the porosity and transport coefficient.

### 3.1. The Broadbalk winter wheat experiment

Figure 2 compares the porosity and diffusion coefficient (average + SE) of the aggregates under different treatments. The most intriguing result is that the porosity and diffusion coefficient of the aggregates in the plot fertilized with farmyard manure were very close to the aggregates taken from the naturalized woodland. In contrast, for chemically fertilized and unfertilized plots, the porosity and diffusion coefficient of their aggregates were comparable. Compared with chemical fertilizations, fertilizing with farmyard manure or returning the soil to natural woodland increased the aggregate porosity and diffusion coefficient by 73% and 159%, and 53% and 115%, respectively.

Aggregates taken from the same plot were heterogeneous, with their effective diffusion coefficient increasing with their porosity approximately in a power law. A visual examination found that the change in diffusion coefficient with porosity for all aggregates can be roughly divided into two groups: one for aggregates taken from unfertilized and chemically fertilized plots, and the other group for those taken from the farmyard manure and the woodland plots. Instead of fitting the porosity-diffusion coefficient relationship for each treatment separately, we fitted the data in the two groups into two power-law functions as shown in Figure 3. The diffusion coefficient increased with porosity faster for aggregates taken from the woodland and farmyard manure plots than for those sampled from the unfertilized and chemically fertilized plots.

### 3.2. The Highfield Ley-Arable experiment

Figure 4 shows the porosity and effective diffusion coefficient of the aggregates sampled from the three plots under different cropping systems. Conversion to arable and bare fallow from a previous grassland changed the intra-aggregate structures and their ability to transport dissolved substrates. The conversion also rendered the aggregates more heterogeneous, especially the bare fallow as the standard errors of the porosity and effective diffusion coefficients of its aggregates are both higher than that for the arable and the grassland. Removing vegetation in the bare fallow developed aggregates which were less porous and permeable. Compared to the continuing grassland, fallowing the soil reduced the porosity and effective diffusion coefficient of the aggregates by 58% and 67% respectively.

As in the wheat experiment, both porosity and effective diffusion coefficient of the aggregates taken from the same plot varied between the aggregate. We fitted the porosity-diffusion coefficient relationship for the aggregates taken from the same plot to a power-law function to elucidate if they trend in the same way (Figure 5). It is manifest that the diffusion coefficient of the aggregates in the arable and grassland plots increased with their porosity approximately in a similar way, deviating from that for the bare fallow plot. As the diffusion coefficient of a soil is modulated by its pore geometry, the above deviation implies that evolution of the intra-aggregate structure is strongly affected by plant-induced microbial activity because the opportunity for roots to penetrate into the aggregates was low.

### 3.3. Diffusion coefficient and soil organic matter

The initial aim of imaging the soils was to investigate their structural change, and soil organic carbon content in each aggregate was not measured. As an approximation, we used the bulk soil total organic carbon (SOC) content from the e-RA database (http://www.era.rothamsted.ac.uk) in the following analysis. We pooled the results for all treatments on the two experiments. In the Broadbalk experiment, the SOC in the top 0-23 cm in 1884 was approximately 30 Mg/ha. Following the fertilization changes, the SOC stabilized approximately 100 years after inception of the experiment. The SOC in the farmyard manure treatment increased to 75 Mg/ha while in the unfertilized treatment, it decreased to 25 Mg/ha, with SOC in plots with chemical fertilizations not showing noticeable changes. In the ley-arable experiment, the SOC under bare fallow, arable land and grassland was 1.34 Mg/ha, 3.42 Mg/ha and 5.8 Mg/ha, respectively.

The SOC content in each treatment was an average (Gregory et al., 2016; Poulton et al., 2018), and Figure 6 plots its relationship with the effective diffusion coefficient of the associated aggregates in all treatments. A positive correlation exists between them, with effective diffusion coefficient of dissolved oxygen in the aggregates increasing with SOC asymptotically - plateauing when SOC exceeds a threshold. Their relationship can be fitted to $D' = \alpha\left[1.0 - \exp\left(-\beta \cdot SOC\right)\right]$, where *SOC* represents the SOC content, and α and β are fitting parameters. The results in Figure 6 are bulk soil SOC rather than SOC in the aggregates. Since the litter content in the woodland is greater than that in other plots, including the woodland aggregates (the blue line) or excluding them (the black line) results in two different fitting curves as shown in Figure 6.

## 4. Discussion

Changes in agronomic practices disturb microbial metabolisms and reshape soil structure, thereby altering SOM as a result. While abiotic and biotic factors influencing this alternation have been intensively studied, their inadequate representation in carbon models is believed to be one reason behind the uncertainties associated with their prediction of the feedback between terrestrial systems and climate change (Tang and Riley, 2015; Koven et al., 2017). Particularly, the microscopic soil structure is crudely parameterized in these models despite its imperative role in biogeochemical processes which underpin carbon cycle (Mueller et al., 2017; Kraychenko et al., 2019). Based on X-ray CT imaging and pore-scale simulation, our results showed how changes in fertilization and cropping system have reshaped intra-aggregate structure, its ability to transport oxygen, as well as the consequence for SOC stabilisation (Figure 6).

We did not measure SOM and organo-mineral complexes in the scanned aggregates because the initial purpose was to investigate soil structural change; we hence used bulk SOC as a proxy. While this is a shortcoming, it is a rational approximation as aggregates are formed microbially in the proximity of plant residuals (Mueller et al., 2017), and around 90% of SOC is found inside the aggregates (Totsche et al., 2018). For organo-mineral complexes, there is mounting evidence that they are proportional to total SOC at a high significant level (Cornelis et al., 2018; Yu et al., 2020).

**4.1. Intra-aggregate structure**

Since the history of the two experiments differs, we analysed their results separately rather than pooling them, however, some common phenomena emerged. Adding organic matter to soil via manure application or plant residues enhanced soil aggregation, but the relative significance of one over the other is largely elusive. Our results showed that planting with or without fertilization increases intra-aggregate porosity and its transport ability compared to the long-term bare fallow (Figures 2-5), especially when fertilized with farmyard manure. This is consistent with some recent findings (Lu et al., 2019; He et al., 2020) but contrary to one (Yu et al., 2020) which showed that long-term manure application densified soil and reduced its transport ability. One possible reason is that the organo-mineral complexes from manure application in the experiment of Yu et al (2020) increased short-range-ordered (SRO) minerals by 20 times, compared to the two-fold increase in SRO minerals in our FYM plot (Yu et al., 2017). Aggregates formed by adsorption and co-precipitation of carbon with SRO minerals appear to be denser than those formed by decomposed organic matter (Crawford et al., 2012; Rabbi et al., 2020).

Effective diffusion coefficient of aggregates depends on how pores of different sizes are spatially arranged, and the way their effective diffusion coefficient trends with their porosity can be used to differentiate aggregates between the treatments (Li et al., 2017). Based on this, we classified the aggregates in each of the two experiments into two groups: bare-fallow group and planting-group for the Highfield ley-arable experiment (Figures 2-3), and FYM-woodland group and chemical fertilization group (including zero-fertilization) for the Broadbalk winter wheat experiment (Figures 4-5). For each experiment, the two groups differed from each other significantly ($p<0.05$). Since roots prefer to go through loose soil and/or large pores (Atkinson et al., 2020; Zhou et al., 2020), they were less likely to have penetrated the aggregates. Therefore, the difference in intra-aggregate structures between the treatments is likely to be dominated by microbial processes. The similarity between intra-aggregate structures and their ability to diffuse substrates for the group under chemical fertilization implies that the intra-aggregate structure was impacted by the quality of roots and root exudates more than by their quantity as wheat biomass under chemical fertilization was much higher than that under the unfertilized treatment (Jenkinson, 1991). This is also corroborated by the results in the ley-arable experiment, where the porosity-diffusion coefficient relationship for the arable and grassland treatments trends more closely than for the bare fallow treatment (Figure 3), although their absolute values differ (Figure 2).

Deviation of the porosity-diffusion coefficient relationship for the FYM treatment from those for the chemical fertilizations means that the manure introduces other mechanisms that helped reshape the intra-aggregate structure. The increased organo-mineral complexes and microbial activity are two of the mechanisms that are already known (Clark et al., 2012; Yu et al., 2017), while others, if there are any, remain obscure.

### 4.2. Soil structure and organic matter

Increasing organic matter input and keeping soil aerobic have been found to enhance soil aggregation and carbon content in aggregates in a wheat-rice rotated paddy field (Huang et al., 2018), but how redox fluctuation impacts aggregate turnover and SOM in soils is less understood. Experiments reported in the literature showed that manure application and conversion to grassland increase SOM, but there is no consensus on their consequence for intra-aggregate structure (Poulton et al., 2003; Poulton et al., 2018). Manure application in our experiment increased transport ability of the aggregates and SOC (Figures 4-5). A decrease in transport ability means it is difficult for substrates and enzymes to move in the aggregates, which would slow down metabolic reactions and lead to carbon accumulation as a result (Davidson et al., 2006). This can account for the results of Yu et al (2020) but is inconsistent with ours and others (Lu et al., 2019; He et al., 2020), which reveal that SOC increased with transport ability of the aggregates.

Traditional pool-based carbon models such as RothC implicitly represent the impact of soil structure using, for example, clay content (Guo et al., 2007). They use a humified SOM pool to collectively describe the organo-mineral complexes and other less-accessible SOM (Guo et al., 2007). Such approaches mathematically capture the reduced decomposition due to the increased inaccessibility, but miss the underlying mechanisms as the carbon immobilised in organo-mineral complexes might become mobile again for microbes to assimilate and respire when the surrounding physicochemical environment in soil changes by, for example, microbial dissimilatory reduction or root exudates (Keiluweit et al., 2015; Yu et al., 2017). Using a humified pool is thus unable to describe this reversible pathway; this is consistent with meta-analysis that SOC depends weakly on clay content but is correlated strongly with Fe and Al (Rasmussen et al., 2018).

SOC in the chemically fertilized arable plot in the ley-arable experiment was greater than that in the chemically fertilized plots in the wheat experiment although the soil texture on the two sites is the same. This is because SOC in the former has not yet reached new equilibria with SOC in the arable plot continuing to decline while that in the grassland is asymptotically increasing. This implicates that aggregate reconstruction following an agronomical practice change is a slow process, corroborated by other research (Totsche et al., 2018; Bacq-Labreuil et al., 2020). Notwithstanding this, metagenomics analysis for the ley-arable experiment indeed found that aerobic-related genes are most abundant in the aggregates taken from the grassland and least in the aggregates taken from the bare fallow, with the arable treatment in between (Neal et al., 2020). This again proves that the transport ability of the aggregates and SOC are positively correlated in the soils.

Our findings suggest that the aggregate transport ability increases asymptotically with SOC, which is consistent with the C-saturation conjecture (Six et al., 2002) although the plateau does not show if the woodland data is excluded. The C-saturation concept is based on an assumption that the reactive mineral surfaces are limited (Six et al., 2002). However, recent work found that SOM between the organo-mineral interface and the organo-organic interface is layered with the organo-mineral interface adsorbing more nitrogen-enriched organic molecules (Possinger et al., 2020). If this is generally true for all mineral soils, the potential capacity of soil minerals to immobilize carbon could be much higher than predicted from the reactive mineral surfaces.

## 5. CONCLUSIONS

Changes in agricultural management and fertilizations had reshaped the intra-aggregate structure and altered SOC content of soil aggregates. Intra-aggregate structures in soil fertilized with farmyard mature were comparable to that in the naturalized woodland, while chemical fertilization did not result in a noticeable change in intra-aggregate structure compared to no-fertilization. Aggregates under the same treatment are heterogeneous, and effective diffusion coefficient of the aggregates in vegetated soils trends with their porosity much differently from that for the bare fallow soil.

A positive correlation was found between SOC and effective diffusion coefficient of the aggregates, proving our conjecture that enhancing stable SOC in unsaturated soils needs the aggregates to be more aerobic. However, the effective diffusion coefficient increases with SOC asymptotically, plateauing when SOC content exceeds a threshold. This is consistent with the C-saturation theory although the plateau does not appear in our results if the woodland data is excluded.

**Appendix A**

Dissolved oxygen diffusion through water in the pore space was simulated using the lattice Boltzmann (LB) model we previously developed (Zhang et al., 2016b; Li et al., 2018) by tracking the movement and collision of a number of fictitious particles. Unlike for fluid flow, the LB model for oxygen diffusion only considers mass balance and we hence use the following single-relaxation approach(Zhang et al., 2016a):

$$f_i\left(\boldsymbol{x}+\delta t\boldsymbol{e}_i, t+\delta t\right)=f_i\left(\boldsymbol{x},t\right)+\frac{1}{\tau}\left[f_i^{eq}\left(\boldsymbol{x},t\right)-f_i\left(\boldsymbol{x},t\right)\right], \tag{A1}$$

where $f_i\left(\boldsymbol{x},t\right)$ is the distribution function for particles at location $\boldsymbol{x}$ and time $t$ moving with lattice velocity $\boldsymbol{e}_i$, $\delta x$ is the side-size of the voxels, $\delta t$ is a time step, $f_i^{eq}\left(\boldsymbol{x},t\right)$ is the associated equilibrium distribution function, and $\tau$ is a relation parameter controlling the collision between the particles and is therefore related to the diffusion coefficient. Since oxygen diffusion in water is isotropic, we use the D3Q7 lattice restricting particles to move in seven directions: $(0,\ 0,\ 0)$, $(\pm\delta x/\delta t,\ 0,\ 0)$ and $(0,\ 0, \pm\delta x/\delta t)$. The equilibrium distribution function associated with each direction is defined by $f_i^{eq}\left(\boldsymbol{x},t\right)=c\left(\boldsymbol{x},t\right)/7,$ where $c\left(\boldsymbol{x},t\right)$ is the concentration at voxel located at $\boldsymbol{x}$ and is calculated during the simulation from

$$c\left(\boldsymbol{x},t\right)=\sum_{i=0}^{6} f_i^{eq}\left(\boldsymbol{x},t\right)=\sum_{i=0}^{6} f_i\ \left(\boldsymbol{x},t\right). \tag{A2}$$

The molecular diffusion coefficient of the dissolved oxygen is associated with the relaxation parameter $\tau$ in $D=2\delta x^2\left(\tau-0.5\right)/7\delta t$

In the LB simulation, advancing one time-step needs two stages. The first one is to calculate the collision part as $f_i^*=f_i\left(\boldsymbol{x},t\right)+\tau^{-1}\left[f_i^{eq}\left(\boldsymbol{x},t\right)-f_i\left(\boldsymbol{x},t\right)\right]$, and the second one is to move the post-collision result $f_i^*$ to $\boldsymbol{x}+\delta t\boldsymbol{e}_i$ to become $f_i\left(\boldsymbol{x}+\delta t\boldsymbol{e}_i, t+\delta t\right)$. In the second stage, whenever a particle hits a pore wall, it is bounced back to where it emanates to reflect that the pore wall is impermeable. In the above LB model, the diffusive flux vector of the oxygen in each voxel is calculated from

$$\boldsymbol{j}(\boldsymbol{x},\ t)=(1-0.5/\tau)\sum_{i=0}^{7} f_i(\boldsymbol{x},t)\boldsymbol{e}_i. \tag{A3}$$

Oxygen diffusion through the water in the pore space is driven by a concentration gradient generated in one direction by imposing a high and a low concentration on the two opposite sides of the sample respectively. The constant concentration boundary is solved using the method we previously proposed (Zhang et al., 2002). The diffusion was simulated to steady state - deemed to have reached once the relative errors between diffusive fluxes calculated at two time points spanning 300 time-steps was less than $10^{-6}$ for all voxels. When diffusion was at steady state, both concentration and diffusive flux at all voxels were sampled to calculate the effective diffusion coefficient as detailed in the main text.

## Acknowledgements

This work forms part of the soils to nutrition (S2N) strategic programme (BBS/E/C/000I0310) funded by the Biotechnology and Biological Sciences Research Council (BBSRC) of the UK. It is also funded by the Natural Environmental Research Council of the UK (NE/T010487/1). The Rothamsted Long-Term Experiments and the Electronic Rothamsted Archive (e-RA) are supported as a BBSRC-funded National Capability (BBS/E/C/000J0300). The authors acknowledge the technique expertise in the X-ray imaging work of Dr Craig Sturrock and Dr Brian Atkinson from the Hounsfield Facility at the University of Nottingham.

## References

Arndt, S., Jorgensen, B.B., LaRowe, D.E., Middelburg, J.J., Pancost, R.D., Regnier, P., 2013. Quantifying the degradation of organic matter in marine sediments: A review and synthesis. Earth-Sci. Rev. 123, 53-86.

Atkinson, J.A., Hawkesford, M.J., Whalley, W.R., Zhou, H., Mooney, S.J., 2020. Soil strength influences wheat root interactions with soil macropores. Plant Cell Environ. 43(1), 235-245.

Bacq-Labreuil, A., Crawford, J., Mooney, S.J., Neal, A.L., Akkari, E., McAuliffe, C., Zhang, X.X., Redmile-Gordon, M., Ritz, K., 2018. Effects of cropping systems upon the three-dimensional architecture of soil systems are modulated by texture. Geoderma 332, 73-83.

Bacq-Labreuil, A., Crawford, J., Mooney, S.J., Neal, A.L., Ritz, K., 2020. Recovery of soil structure under long-term fallow in response to annual or perennial cropping requires at least 10 years after conversion. Enropean Journal of Soil Science 9, 9.

Baldock, J.A., Skjemstad, J.O., 2000. Role of the soil matrix and minerals in protecting natural organic materials against biological attack. Org. Geochem. 31(7-8), 697-710.
Baveye, P.C., Otten, W., Kravchenko, A., Balseiro-Romero, M., Beckers, E., Chalhoub, M., Darnault, C., Eickhorst, T., Garnier, P., Hapca, S., Kiranyaz, S., Monga, O., Mueller, C.W., Nunan, N., Pot, V., Schluter, S., Schmidt, H., Vogel, H.J., 2018. Emergent Properties of Microbial Activity in Heterogeneous Soil Microenvironments: Different Research Approaches Are Slowly Converging, Yet Major Challenges Remain. Front. Microbiol. 9, 48.
Blair, N., Faulkner, R.D., Till, A.R., Poulton, P.R., 2006. Long-term management impacts on soil C, N and physical fertility - Part 1: Broadbalk experiment. Soil Tillage Res. 91(1-2), 30-38.
Bolker, B.M., Pacala, S.W., Parton, W.J., 1998. Linear analysis of soil decomposition: Insights from the century model. Ecol. Appl. 8(2), 425-439.
Boudreau, B.P., Arnosti, C., Jorgensen, B.B., Canfield, D.E., 2008. Comment on "Physical model for the decay and preservation of marine organic carbon". Science 319(5870), 2.
Chakrawal, A., Herrmann, A.M., Koestel, J., Jarsjo, J., Nunan, N., Katterer, T., Manzoni, S., 2020. Dynamic upscaling of decomposition kinetics for carbon cycling models. Geosci. Model Dev. 13(3), 1399-1429.
Chen, C.M., Hall, S.J., Coward, E., Thompson, A., 2020. Iron-mediated organic matter decomposition in humid soils can counteract protection. Nat. Commun. 11(1), 13.
Chenu, C., Angers, D.A., Barre, P., Derrien, D., Arrouays, D., Balesdent, J., 2019. Increasing organic stocks in agricultural soils: Knowledge gaps and potential innovations. Soil Tillage Res. 188, 41-52.
Clark, I.M., Buchkina, N., Jhurreea, D., Goulding, K.W.T., Hirsch, P.R., 2012. Impacts of nitrogen application rates on the activity and diversity of denitrifying bacteria in the Broadbalk Wheat Experiment. Philos. Trans. R. Soc. B-Biol. Sci. 367(1593), 1235-1244.
Cornelis, J.T., Delvaux, B., Van Ranst, E., Rouxhet, P.G., 2018. Sub-micrometer distribution of Fe oxides and organic matter in Podzol horizons. Geoderma 323, 126-135.
Crawford, J.W., Deacon, L., Grinev, D., Harris, J.A., Ritz, K., Singh, B.K., Young, I., 2012. Microbial diversity affects self-organization of the soil-microbe system with consequences for function. J. R. Soc. Interface 9(71), 1302-1310.
Davidson, E.A., Janssens, I.A., Luo, Y.Q., 2006. On the variability of respiration in terrestrial ecosystems: moving beyond Q(10). Glob. Change Biol. 12(2), 154-164.
Davidson, E.A., Samanta, S., Caramori, S.S., Savage, K., 2012. The Dual Arrhenius and Michaelis-Menten kinetics model for decomposition of soil organic matter at hourly to seasonal time scales. Glob. Change Biol. 18(1), 371-384.
DeGryze, S., Six, J., Paustian, K., Morris, S.J., Paul, E.A., Merckx, R., 2004. Soil organic carbon pool changes following land-use conversions. Glob. Change Biol. 10(7), 1120-1132.
Dubinsky, E.A., Silver, W.L., Firestone, M.K., 2010. Tropical forest soil microbial communities couple iron and carbon biogeochemistry. Ecology 91(9), 2604-2612.
Dungait, J.A.J., Hopkins, D.W., Gregory, A.S., Whitmore, A.P., 2012. Soil organic matter turnover is governed by accessibility not recalcitrance. Glob. Change Biol. 18(6), 1781-1796.
Ebrahimi, A., Or, D., 2016. Microbial community dynamics in soil aggregates shape biogeochemical gas fluxes from soil profiles - upscaling an aggregate biophysical model. Glob. Change Biol. 22(9), 3141-3156.
Freeman, C., Ostle, N., Kang, H., 2001. An enzymic 'latch' on a global carbon store - A shortage of oxygen locks up carbon in peatlands by restraining a single enzyme. Nature 409(6817), 149-149.
Ghezzehei, T.A., Sulman, B., Arnold, C.L., Bogie, N.A., Berhe, A.A., 2019. On the role of soil water retention characteristic on aerobic microbial respiration. Biogeosciences 16(6), 1187-1209.
Gregory, A.S., Bird, N.R.A., Whalley, W.R., Matthews, G.P., Young, I.M., 2010. Deformation and Shrinkage Effects on the Soil Water Release Characteristic. Soil Sci. Soc. Am. J. 74(4), 1104-1112.

Gregory, A.S., Dungait, J.A.J., Watts, C.W., Bol, R., Dixon, E.R., White, R.P., Whitmore, A.P., 2016. Long-term management changes topsoil and subsoil organic carbon and nitrogen dynamics in a temperate agricultural system. Eur. J. Soil Sci. 67(4), 421-430.

Guber, A., Kraychenko, A., Razavi, B.S., Uteau, D., Peth, S., Blagodatskaya, E., Kuzyakov, Y., 2018. Quantitative soil zymography: Mechanisms, processes of substrate and enzyme diffusion in porous media. Soil Biol. Biochem. 127, 156-167.

Guo, L., Falloon, P., Coleman, K., Zhou, B., Li, Y., Lin, E., Zhang, F., 2007. Application of the RothC model to the results of long-term experiments on typical upland soils in northern China. Soil Use Manage. 23(1), 63-70.

Hall, S.J., Silver, W.L., 2015. Reducing conditions, reactive metals, and their interactions can explain spatial patterns of surface soil carbon in a humid tropical forest. Biogeochemistry 125(2), 149-165.

Harris, E., Diaz-Pines, E., Stoll, E., Schloter, M., Schulz, S., Duffner, C., Li, K., Moore, K.L., Ingrisch, J., Reinthaler, D., Zechmeister-Boltenstern, S., Glatzel, S., Brüggemann, N., Bahn, M., 2021. Denitrifying pathways dominate nitrous oxide emissions from managed grassland during drought and rewetting. Sci. Adv. 7(6), eabb7118.

He, L.L., Zhao, J., Yang, S.M., Zhou, H., Wang, S.Q., Zhao, X., Xing, G.X., 2020. Successive biochar amendment improves soil productivity and aggregate microstructure of a red soil in a five-year wheat-millet rotation pot trial. Geoderma 376, 9.

Hemingway, J.D., Rothman, D.H., Grant, K.E., Rosengard, S.Z., Eglinton, T.I., Derry, L.A., Galy, V.V., 2019. Mineral protection regulates long-term global preservation of natural organic carbon. Nature 570(7760), 228-+.

Huang, W.J., Ye, C.L., Hockaday, W.C., Hall, S.J., 2020. Trade-offs in soil carbon protection mechanisms under aerobic and anaerobic conditions. Glob. Change Biol. 26(6), 3726-3737.

Huang, X.L., Tang, H.Y., Kang, W.J., Yu, G.H., Ran, W., Hong, J.P., Shen, Q.R., 2018. Redox interface-associated organo-mineral interactions: A mechanism for C sequestration under a rice-wheat cropping system. Soil Biol. Biochem. 120, 12-23.

Jenkinson, D.S., 1991. THE ROTHAMSTED LONG-TERM EXPERIMENTS - ARE THEY STILL OF USE. Agron. J. 83(1), 2-10.

Jensen, J.L., Schjonning, P., Watts, C.W., Christensen, B.T., Peltre, C., Munkholm, L.J., 2019. Relating soil C and organic matter fractions to soil structural stability. Geoderma 337, 834-843.

Jones, E., Singh, B., 2014. Organo-mineral interactions in contrasting soils under natural vegetation. Frontiers in Environmental Science 2(2).

Keiluweit, M., Bougoure, J.J., Nico, P.S., Pett-Ridge, J., Weber, P.K., Kleber, M., 2015. Mineral protection of soil carbon counteracted by root exudates. Nat. Clim. Chang. 5(6), 588-595.

Keiluweit, M., Nico, P.S., Kleber, M., Fendorf, S., 2016. Are oxygen limitations under recognized regulators of organic carbon turnover in upland soils? Biogeochemistry 127(2-3), 157-171.

Knorr, K.H., 2013. DOC-dynamics in a small headwater catchment as driven by redox fluctuations and hydrological flow paths - are DOC exports mediated by iron reduction/oxidation cycles? Biogeosciences 10(2), 891-904.

Kogel-Knabner, I., Guggenberger, G., Kleber, M., Kandeler, E., Kalbitz, K., Scheu, S., Eusterhues, K., Leinweber, P., 2008. Organo-mineral associations in temperate soils: Integrating biology, mineralogy, and organic matter chemistry. J. Plant Nutr. Soil Sci. 171(1), 61-82.

Koven, C.D., Hugelius, G., Lawrence, D.M., Wieder, W.R., 2017. Higher climatological temperature sensitivity of soil carbon in cold than warm climates. Nat. Clim. Chang. 7(11), 817-+.

Kraychenko, A.N., Guber, A.K., Razavi, B.S., Koestel, J., Quigley, M.Y., Robertson, G.P., Kuzyakov, Y., 2019. Microbial spatial footprint as a driver of soil carbon stabilization. Nature Communications 10, 10.

LaRowe, D.E., Van Cappellen, P., 2011. Degradation of natural organic matter: A thermodynamic analysis. Geochim. Cosmochim. Acta 75(8), 2030-2042.

Lehmann, J., Hansel, C.M., Kaiser, C., Kleber, M., Maher, K., Manzoni, S., Nunan, N., Reichstein, M., Schimel, J.P., Torn, M.S., Wieder, W.R., Kogel-Knabner, I., 2020. Persistence of soil organic carbon caused by functional complexity. Nature Geoscience 13(8), 529-534.

Lehmann, J., Kleber, M., 2015. The contentious nature of soil organic matter. Nature 528(7580), 60-68.

Li, Z.Y., Zhang, X.X., Liu, Y., 2017. Pore-scale simulation of gas diffusion in unsaturated soil aggregates: Accuracy of the dusty-gas model and the impact of saturation. Geoderma 303, 196-203.

Li, Z.Y., Zhang, X.X., Wang, D., Liu, Y., 2018. Direct methods to calculate the mass exchange between solutes inside and outside aggregates in macroscopic model for solute transport in aggregated soil. Geoderma 320, 126-135.

Lu, S.G., Yu, X.L., Zong, Y.T., 2019. Nano-microscale porosity and pore size distribution in aggregates of paddy soil as affected by long-term mineral and organic fertilization under rice-wheat cropping system. Soil Tillage Res. 186, 191-199.

Lucas, M., Pihlap, E., Steffens, M., Vetterlein, D., Kogel-Knabner, I., 2020. Combination of Imaging Infrared Spectroscopy and X-ray Computed Microtomography for the Investigation of Bio- and Physicochemical Processes in Structured Soils. Front. Environ. Sci. 8, 12.

Luo, Y.Q., Ahlstrom, A., Allison, S.D., Batjes, N.H., Brovkin, V., Carvalhais, N., Chappell, A., Ciais, P., Davidson, E.A., Finzi, A.C., Georgiou, K., Guenet, B., Hararuk, O., Harden, J.W., He, Y.J., Hopkins, F., Jiang, L.F., Koven, C., Jackson, R.B., Jones, C.D., Lara, M.J., Liang, J.Y., McGuire, A.D., Parton, W., Peng, C.H., Randerson, J.T., Salazar, A., Sierra, C.A., Smith, M.J., Tian, H.Q., Todd-Brown, K.E.O., Torn, M., van Groenigen, K.J., Wang, Y.P., West, T.O., Wei, Y.X., Wieder, W.R., Xia, J.Y., Xu, X., Xu, X.F., Zhou, T., 2016. Toward more realistic projections of soil carbon dynamics by Earth system models. Glob. Biogeochem. Cycle 30(1), 40-56.

Luo, Z.K., Rossel, R.A.V., Shi, Z., 2020. Distinct controls over the temporal dynamics of soil carbon fractions after land use change. Glob. Change Biol. 26(8), 4614-4625.

Manzoni, S., Pineiro, G., Jackson, R.B., Jobbagy, E.G., Kim, J.H., Porporato, A., 2012. Analytical models of soil and litter decomposition: Solutions for mass loss and time-dependent decay rates. Soil Biol. Biochem. 50, 66-76.

Moyano, F.E., Manzoni, S., Chenu, C., 2013. Responses of soil heterotrophic respiration to moisture availability: An exploration of processes and models. Soil Biol. Biochem. 59, 72-85.

Mueller, C.W., Hoeschen, C., Steffens, M., Buddenbaum, H., Hinkel, K., Bockheim, J.G., Kao-Kniffin, J., 2017. Microscale soil structures foster organic matter stabilization in permafrost soils. Geoderma 293, 44-53.

Neal, A.L., Bacq-Labreuil, A., Zhang, X.X., Clark, I.M., Coleman, K., Mooney, S.J., Ritz, K., Crawford, J.W., 2020. Soil as an extended composite phenotype of the microbial metagenome. Sci Rep 10(1), 16.

Nunan, N., Wu, K.J., Young, I.M., Crawford, J.W., Ritz, K., 2003. Spatial distribution of bacterial communities and their relationships with the micro-architecture of soil. FEMS Microbiol. Ecol. 44(2), 203-215.

Possinger, A.R., Zachman, M.J., Enders, A., Levin, B.D.A., Muller, D.A., Kourkoutis, L.F., Lehmann, J., 2020. Organo–organic and organo–mineral interfaces in soil at the nanometer scale. Nat. Commun. 11(1), 6103.

Poulton, P., Johnston, J., Macdonald, A., White, R., Powlson, D., 2018. Major limitations to achieving "4 per 1000" increases in soil organic carbon stock in temperate regions: Evidence from long-term experiments at Rothamsted Research, United Kingdom. Glob. Change Biol. 24(6), 2563-2584.

Poulton, P.R., Pye, E., Hargreaves, P.R., Jenkinson, D.S., 2003. Accumulation of carbon and nitrogen by old arable land reverting to woodland. Glob. Change Biol. 9(6), 942-955.

Rabbi, S.M.F., Minasny, B., McBratney, A.B., Young, L.M., 2020. Microbial processing of organic matter drives stability and pore geometry of soil aggregates. Geoderma 360, 4.

Rabot, E., Wiesmeier, M., Schluter, S., Vogel, H.J., 2018. Soil structure as an indicator of soil functions: A review. Geoderma 314, 122-137.
Rasmussen, C., Heckman, K., Wieder, W.R., Keiluweit, M., Lawrence, C.R., Berhe, A.A., Blankinship, J.C., Crow, S.E., Druhan, J.L., Pries, C.E.H., Marin-Spiotta, E., Plante, A.F., Schadel, C., Schimel, J.P., Sierra, C.A., Thompson, A., Wagai, R., 2018. Beyond clay: towards an improved set of variables for predicting soil organic matter content. Biogeochemistry 137(3), 297-306.
Redmile-Gordon, M., Gregory, A.S., White, R.P., Watts, C.W., 2020. Soil organic carbon, extracellular polymeric substances (EPS), and soil structural stability as affected by previous and current land-use. Geoderma 363, 10.
Rothman, D.H., Forney, D.C., 2007. Physical model for the decay and preservation of marine organic carbon. Science 316(5829), 1325-1328.
Schmidt, M.W.I., Torn, M.S., Abiven, S., Dittmar, T., Guggenberger, G., Janssens, I.A., Kleber, M., Kogel-Knabner, I., Lehmann, J., Manning, D.A.C., Nannipieri, P., Rasse, D.P., Weiner, S., Trumbore, S.E., 2011. Persistence of soil organic matter as an ecosystem property. Nature 478(7367), 49-56.
Schneider, C.A., Rasband, W.S., Eliceiri, K.W., 2012. NIH Image to ImageJ: 25 years of image analysis. Nat. Methods 9(7), 671-675.
Sexstone, A.J., Revsbech, N.P., Parkin, T.B., Tiedje, J.M., 1985. DIRECT MEASUREMENT OF OXYGEN PROFILES AND DENITRIFICATION RATES IN SOIL AGGREGATES. Soil Sci. Soc. Am. J. 49(3), 645-651.
Six, J., Conant, R.T., Paul, E.A., Paustian, K., 2002. Stabilization mechanisms of soil organic matter: Implications for C-saturation of soils. Plant Soil 241(2), 155-176.
Skopp, J., Jawson, M.D., Doran, J.W., 1990. Steady-state aerobic microbial activity as a function of soil water content Soil Sci. Soc. Am. J. 54(6), 1619-1625.
Smith, P., Soussana, J.F., Angers, D., Schipper, L., Chenu, C., Rasse, D.P., Batjes, N.H., van Egmond, F., McNeill, S., Kuhnert, M., Arias-Navarro, C., Olesen, J.E., Chirinda, N., Fornara, D., Wollenberg, E., Alvaro-Fuentes, J., Sanz-Cobena, A., Klumpp, K., 2020. How to measure, report and verify soil carbon change to realize the potential of soil carbon sequestration for atmospheric greenhouse gas removal. Glob. Change Biol. 26(1), 219-241.
Soussana, J.F., Lutfalla, S., Ehrhardt, F., Rosenstock, T., Lamanna, C., Havlik, P., Richards, M., Wollenberg, E., Chotte, J.L., Torquebiau, E., Ciais, P., Smith, P., Lal, R., 2019. Matching policy and science: Rationale for the '4 per 1000-soils for food security and climate' initiative. Soil Tillage Res. 188, 3-15.
Sulman, B.N., Phillips, R.P., Oishi, A.C., Shevliakova, E., Pacala, S.W., 2014. Microbe-driven turnover offsets mineral-mediated storage of soil carbon under elevated CO2. Nat. Clim. Chang. 4(12), 1099-1102.
Sutton, R., Sposito, G., 2005. Molecular structure in soil humic substances: The new view. Environ. Sci. Technol. 39(23), 9009-9015.
Sykes, A.J., Macleod, M., Eory, V., Rees, R.M., Payen, F., Myrgiotis, V., Williams, M., Sohi, S., Hillier, J., Moran, D., Manning, D.A.C., Goglio, P., Seghetta, M., Williams, A., Harris, J., Dondini, M., Walton, J., House, J., Smith, P., 2020. Characterising the biophysical, economic and social impacts of soil carbon sequestration as a greenhouse gas removal technology. Glob. Change Biol. 26(3), 1085-1108.
Tang, J.Y., Riley, W.J., 2015. Weaker soil carbon-climate feedbacks resulting from microbial and abiotic interactions. Nat. Clim. Chang. 5(1), 56-60.
Totsche, K.U., Amelung, W., Gerzabek, M.H., Guggenberger, G., Klumpp, E., Knief, C., Lehndorff, E., Mikutta, R., Peth, S., Prechtel, A., Ray, N., Kogel-Knabner, I., 2018. Microaggregates in soils. J. Plant Nutr. Soil Sci. 181(1), 104-136.
van Groenigen, J.W., van Kessel, C., Hungate, B.A., Oenema, O., Powlson, D.S., van Groenigen, K.J., 2017. Sequestering Soil Organic Carbon: A Nitrogen Dilemma. Environ. Sci. Technol. 51(9), 4738-4739.

Vogel, H.J., Kretzschmar, A., 1996. Topological characterization of pore space in soil - Sample preparation and digital image-processing. Geoderma 73(1-2), 23-38.
von Lutzow, M., Kogel-Knabner, I., Ekschmitt, K., Matzner, E., Guggenberger, G., Marschner, B., Flessa, H., 2006. Stabilization of organic matter in temperate soils: mechanisms and their relevance under different soil conditions - a review. Eur. J. Soil Sci. 57(4), 426-445.
Wang, Y.Y., Wang, H., He, J.S., Feng, X.J., 2017. Iron-mediated soil carbon response to water-table decline in an alpine wetland. Nat. Commun. 8, 9.
Watts, C.W., Clark, L.J., Poulton, P.R., Powlson, D.S., Whitmore, A.P., 2006. The role of clay, organic carbon and long-term management on mouldboard plough draught measured on the Broadbalk wheat experiment at Rothamsted. Soil Use Manage. 22(4), 334-341.
Yan, Z.F., Bond-Lamberty, B., Todd-Brown, K.E., Bailey, V.L., Li, S.L., Liu, C.Q., Liu, C.X., 2018. A moisture function of soil heterotrophic respiration that incorporates microscale processes. Nat. Commun. 9, 10.
Young, I.M., Crawford, J.W., 2004. Interactions and self-organization in the soil-microbe complex. Science 304(5677), 1634-1637.
Yu, G.H., Chen, C.M., He, X.H., Zhang, X.Z., Li, L.N., 2020. Unexpected bulk density and microstructures response to long-term pig manure application in a Ferralic Cambisol Soil: Implications for rebuilding a healthy soil. Soil Tillage Res. 203, 8.
Yu, G.H., Xiao, J., Hu, S.J., Polizzotto, M.L., Zhao, F.J., McGrath, S.P., Li, H., Ran, W., Shen, Q.R., 2017. Mineral Availability as a Key Regulator of Soil Carbon Storage. Environ Sci Technol 51(9), 4960-4969.
Yuan, Y.S., Zhang, Z.L., Chen, L.J., Yang, C., 2020. The formation of protected SOM facilitated by labile C input via artificial roots. Eur. J. Soil Biol. 100, 9.
Zhang, X., Crawford, J.W., Flavel, R.J., Young, I.M., 2016a. A multi-scale Lattice Boltzmann model for simulating solute transport in 3D X-ray micro-tomography images of aggregated porous materials. J. Hydrol. 541, Part B, 1020-1029.
Zhang, X., Neal, A.L., Crawford, J.W., Bacq-Labreuil, A., Akkari, E., Rickard, W., 2021. The effects of long-term fertilizations on soil hydraulic properties vary with scales. J. Hydrol. 593, 125890.
Zhang, X.X., Crawford, J.W., Bengough, A.G., Young, I.M., 2002. On boundary conditions in the lattice Boltzmann model for advection and anisotropic dispersion equation. Advances in Water Resources 25(6), 601-609.
Zhang, X.X., Crawford, J.W., Flavel, R.J., Young, I.M., 2016b. A multi-scale Lattice Boltzmann model for simulating solute transport in 3D X-ray micro-tomography images of aggregated porous materials. J. Hydrol. 541, 1020-1029.
Zhao, Q., Adhikari, D., Huang, R.X., Patel, A., Wang, X.L., Tang, Y.Z., Obrist, D., Roden, E.E., Yang, Y., 2017. Coupled dynamics of iron and iron-bound organic carbon in forest soils during anaerobic reduction. Chem. Geol. 464, 118-126.
Zhao, Q., Dunham-Cheatham, S., Adhikari, D., Chen, C.M., Patel, A., Poulson, S.R., Obrist, D., Verburg, P.S.J., Wang, X.L., Roden, E.R., Thompson, A., Yang, Y., 2020. Oxidation of soil organic carbon during an anoxic-oxic transition. Geoderma 377, 9.
Zhou, H., Whalley, W.R., Hawkesford, M.J., Ashton, R.W., Atkinson, B., Atkinson, J.A., Sturrock, C.J., Bennett, M.J., Mooney, S.J., 2020. The interaction between wheat roots and soil pores in structured field soil. J. Exp. Bot. 72(2), 747-756.

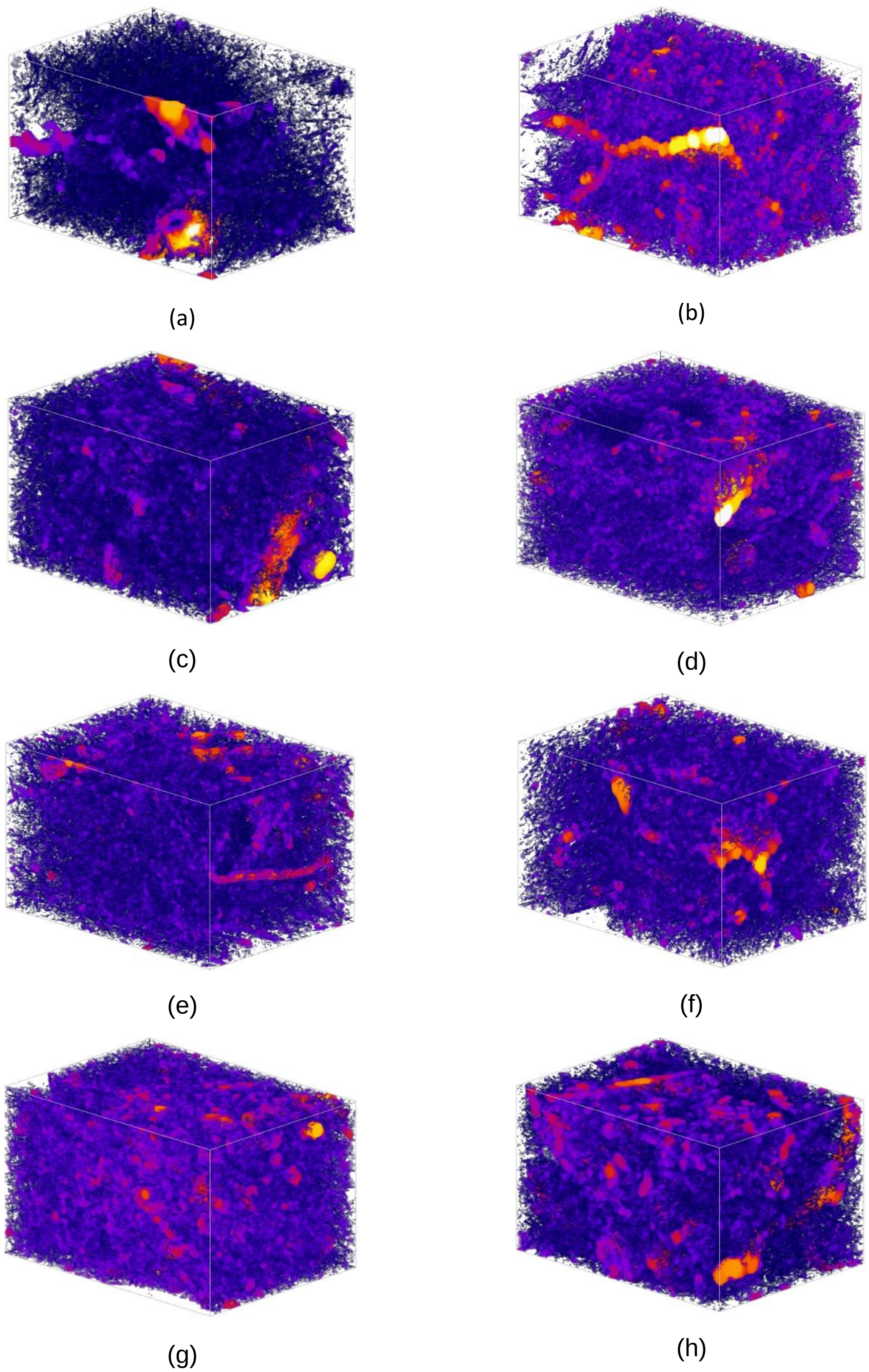


**Figure 1**. Representative aggregate images for soils taken from different treatments. Bare fallow (a), arable (b) and grassland (c) in Highfield Ley-Arable experiment; full chemical fertilization(d), chemical fertilization without P (e), no-fertilization (f), farmyard manure fertilization (g), and Woodland (h) in Broadbalk Winter Wheat experiment.

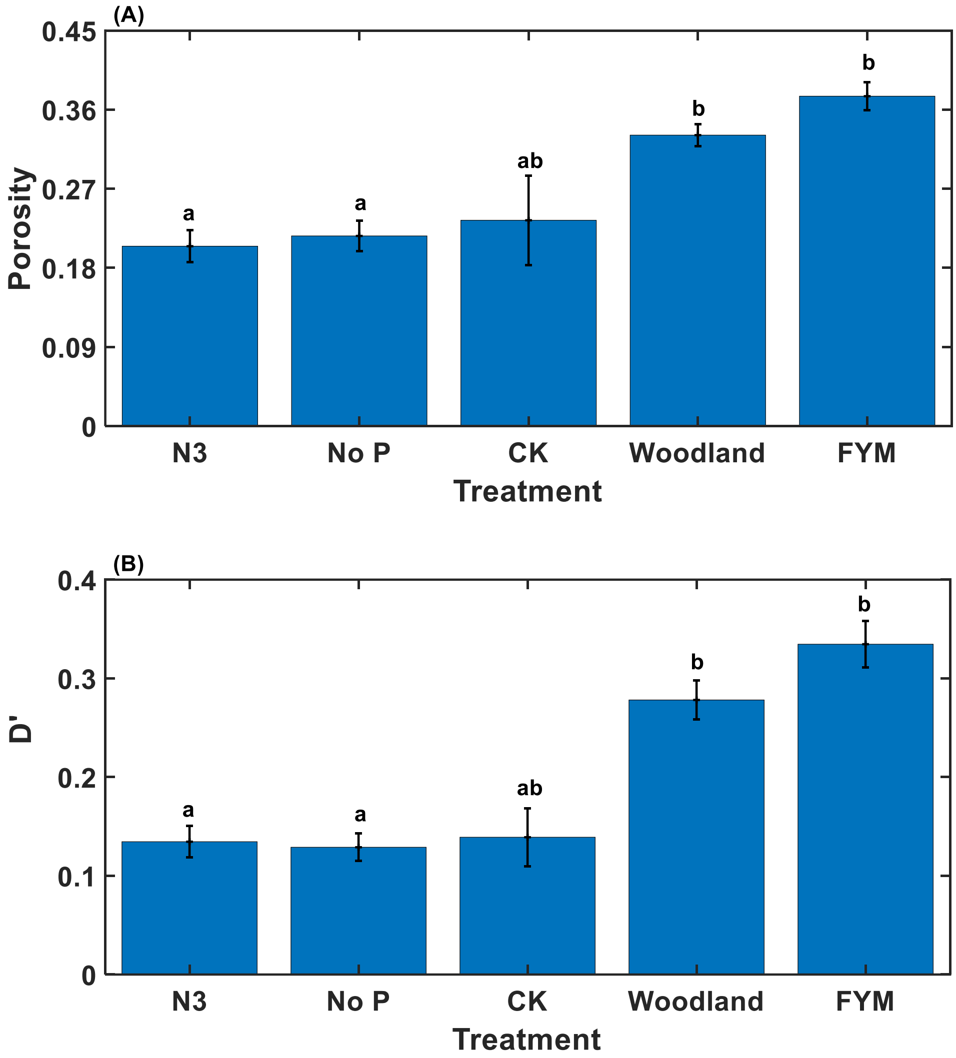


**Figure 2.** Change in average porosity (a) and normalised average effective diffusion coefficient of the aggregates with treatment: Full chemical fertilization (N3), chemical fertilization without P (No P), no-fertilization (CK), Woodland, and farmyard manure fertilization (FYM) in Broadbalk Winter Wheat experiment.

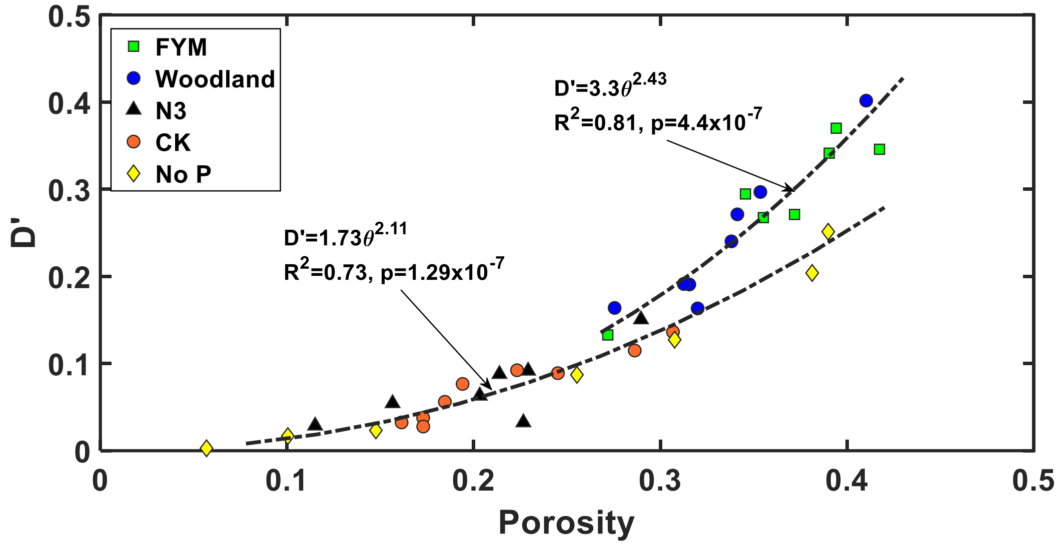


**Figure 3**. Change in the normalised effective diffusion coefficient with porosity for all aggregates taken from soils under full chemical fertilization (N3), chemical fertilization without P (No P), no-fertilization (CK), Woodland and farmyard manure fertilization (FYM) in Broadbalk Winter Wheat experiment (the two solid lines are power-law fitting for woodland + FYM and all other treatments, respectively).

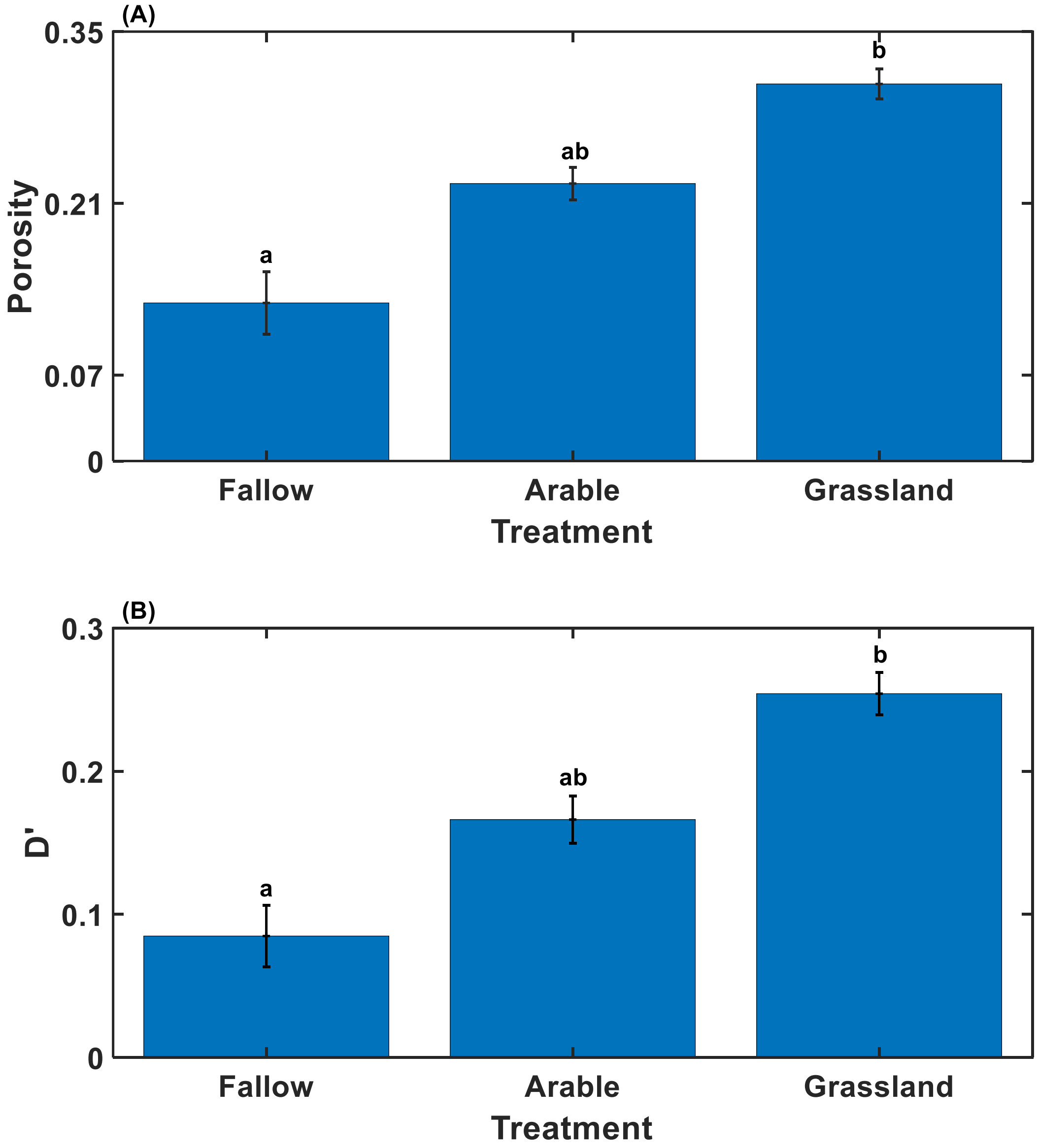


**Figure 4**. Change in average porosity (a) and normalised average effective diffusion coefficient (b) of the aggregates with treatment in Highfield Ley-Arable experiment.

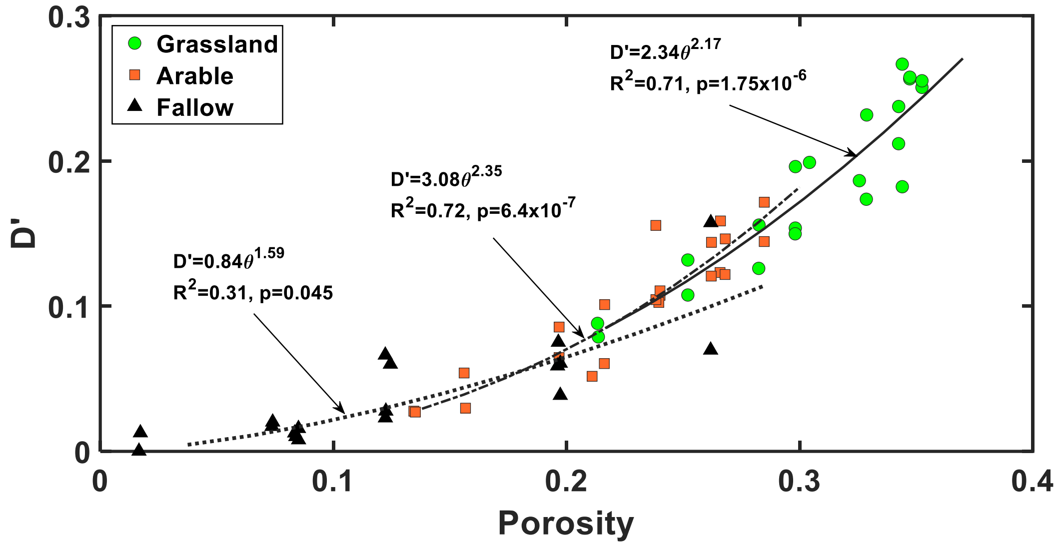


**Figure 5**. Change in normalised effective diffusion coefficient with porosity for all aggregates taken from soils under the three treatments in Highfield Ley-Arable experiment. The solid lines are power-law fitting for each treatment.

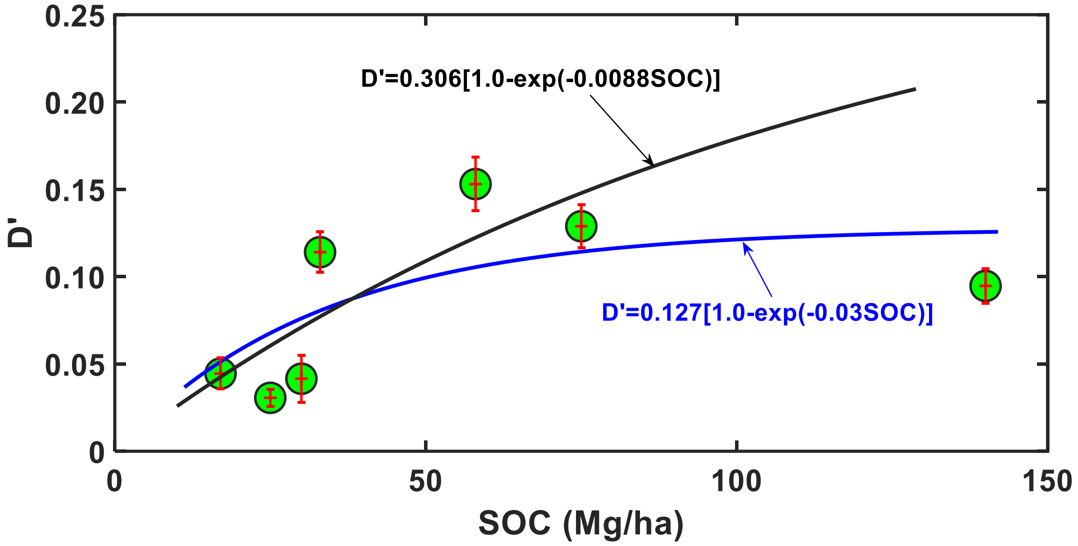


**Figure 6**. Change in normalised effective diffusion coefficient of the aggregates with bulk SOC, with results for Broadbalk Winter Wheat and Highfield Ley-Arable experiments pooled. The blue line is the fitting considering the woodland aggregates and the black line is the fitting without considering them.